PARTICLE FILTERING FOR MULTIPLE OBJECT TRACKING IN MOLECULAR CELL BIOLOGY

Ihor Smal, Wiro Niessen and Erik Meijering

Biomedical Imaging Group Rotterdam
Erasmus MC – University Medical Center Rotterdam
Email: i.smal@erasmusmc.nl

ABSTRACT

Motion analysis of subcellular structures in living cells is currently a major topic in molecular cell biology, for which computerized methods are desperately needed. In this paper we adopt and tailor particle filtering techniques for this purpose and present the results of robust and accurate tracking of multiple objects in real fluorescence microscopy image data acquired for specific biological studies. Experimental results demonstrate that the automated method produces results comparable to manual tracking but using only a fraction of the manual tracking time.

1. INTRODUCTION

Recent advances in molecular biology and fluorescence microscopy imaging make possible the acquisition of multidimensional image data and the observation of the dynamics of intracellular molecular activities. Motion analysis of subcellular structures such as microtubules or proliferating cell nuclear antigen-like proteins (Fig. 1) requires tracking of hundreds of bright spots in noisy image sequences [1]. Contrary to applications where tracking of all objects present in a scene is required, for biologists it is usually sufficient to track only a part of them in order to obtain the necessary statistics about the localization and dynamic behavior.

In a recent paper [2], we have demonstrated the potential of particle filtering (PF) techniques for object tracking in 2D+time and 3D+time bioimaging by using simulated but highly realistic image sequences, for which ground truth was available. The quantitative comparison showed that these probabilistic approaches are more robust to noise for signal-to-noise ratios (SNR) of 2-5 than existing tracking techniques in this area, which separate the object detection and object linking stages and usually break down at SNR$<$5 [3],[4].

In this paper we demonstrate the applicability of PF techniques for real biological applications and show the results of tracking microtubules in 2D image sequences obtained by fluorescence microscopy imaging.

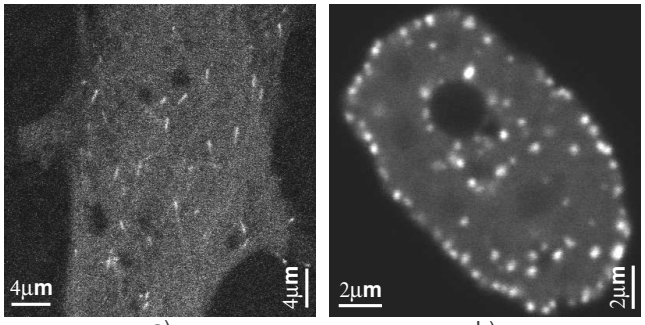

Fig. 1. Examples of a) microtubules labeled with plus end tracking proteins, and b) proliferating cell nuclear antigen proteins, imaged using fluorescence confocal microscopy. The images are single frames from 2D time-lapse studies (Courtesy Drs. Niels Galjart and Jeroen Essers, Erasmus MC).

2. TRACKING FRAMEWORK

Bayesian estimation is used to recursively estimate a time evolving posterior distribution (or filtering distribution) $p(\mathbf{x}_k|\mathbf{z}_{1:k})$ that describes the object state $\mathbf{x}_k$ given all observations $\mathbf{z}_{1:k}$ up to time k. This distribution can be computed by specifying the Markovian probabilistic model of the state evolution $D(\mathbf{x}_k|\mathbf{x}_{k-1})$ and the likelihood $L(\mathbf{z}_k|\mathbf{x}_k)$ of any state having the current observation, and using the two step (prediction and update) recursion [5]:

$$p(\mathbf{x}_k|\mathbf{z}_{1:k-1}) = \int D(\mathbf{x}_k|\mathbf{x}_{k-1})p(\mathbf{x}_{k-1}|\mathbf{z}_{1:k-1})d\mathbf{x}_{k-1}, \quad (1)$$

$$p(\mathbf{x}_k|\mathbf{z}_{1:k}) \propto L(\mathbf{z}_k|\mathbf{x}_k)p(\mathbf{x}_k|\mathbf{z}_{1:k-1}). \quad (2)$$

For practical implementation of the Bayesian approach the condensation algorithm has been used [6]. The filtering distribution in this case is represented with a set of N_s random samples (particles) and associated importance weights $\{\mathbf{x}_k^i, w_k^i\}_{i=1}^{N_s}$, which are then propagated through time to give approximations of the filtering distribution at subsequent time steps. The weights are normalized ($\sum_i w_k^i = 1$) in order to obtain a discrete approximation of the filtering distribution

$$p(\mathbf{x}_k|\mathbf{z}_{1:k}) \approx \sum_{i=1}^{N_s} w_k^i \delta(\mathbf{x}_k - \mathbf{x}_k^i).$$

To capture the multi-modal nature of the data, which is inherent to our application in which tracking of multiple objects is required, the filtering distribution was modeled as an M-component mixture model

$$p(\mathbf{x}_k|\mathbf{z}_{1:k}) = \sum_{m=1}^{M} \pi_m(k) p_m(\mathbf{x}_k|\mathbf{z}_{1:k}) \tag{3}$$

with $\sum_{m=1}^{M} \pi_m(k) = 1$ and a non-parametric model is assumed for the individual mixture components. This non-parametric mixture representation can be updated in the same fashion as the two-step approach for standard Bayesian sequential estimation [5]. This approach allows for a deterministic spatial reclustering procedure, which includes any mixture computation operation of interest: merging, splitting, and reclustering of the tracked objects, which also have a direct analogy with biological phenomena.

3. EXPERIMENTS AND RESULTS

3.1. Microtubule Growth Study

The method was evaluated on 2D image sequences of growing microtubules. Microtubules (MTs) are highly dynamic cylindrical structures (diameter$\sim$25 nm) in the cytoskeleton, consisting of α and β tubulin proteins. Owing to their importance for cell cycle and basal function, current research groups study MTs in terms of structure, localization and dynamic behavior under different experimental conditions such as drug treatment, incubation with MT associated proteins and/or tubulin isoforms. The ends of the microtubules are tagged with +TIPs (plus end tracking proteins) which serve as powerful markers for visualizing microtubule growth events. The images (Fig. 1a) contain hundreds of tags and were taken using fluorescence confocal microscopy. Manual tracking in this case is rather tedious and may yield inaccurate and poorly reproducible results.

3.2. Dynamic Model

To mimic the dynamics of the visible ends of microtubules we adopt a nearly constant velocity model for object motion [7] and a random walk model for object intensity I_k. In this case, the corresponding state-space model, with the state vector $\mathbf{x}_k = (x_k, \dot{x}_k, y_k, \dot{y}_k, I_k)^T$ and zero-mean Gaussian noise $\mathbf{v}_k$ with covariance $\mathbf{Q}$, is given by

$$\mathbf{x}_{k+1} = \mathbf{F}\mathbf{x}_k + \mathbf{v}_k = \text{diag}[\mathbf{F}_1, \mathbf{F}_1, 1]\mathbf{x}_k + \mathbf{v}_k \tag{4}$$

where $\mathbf{Q} = \text{diag}[\mathbf{Q}_1, \mathbf{Q}_1, q_2 T]$,

$$\mathbf{F}_1 = \begin{pmatrix} 1 & T \\ 0 & 1 \end{pmatrix}, \qquad \mathbf{Q}_1 = \begin{pmatrix} \frac{q_1}{3}T^3 & \frac{q_1}{2}T^2 \\ \frac{q_1}{2}T^2 & q_1 T \end{pmatrix}$$

where q_1 and q_2 denote the level of process noise in object motion and intensity, respectively, and T is the sampling interval. This model correctly approximates small accelerations in the object motion and fluctuations in the object intensity present in our image data.

3.3. Observation Model

The measured images are recorded at discrete instants k with a sampling interval T, each image consisting of $N \times M$ pixels. At each pixel (i, j), which corresponds to a rectangular region of dimensions $\Delta_x \times \Delta_y$ nm^2, the measured intensity is denoted as $z_k(i, j)$. Because of the relatively low resolution ($\sim$200nm) of optical microscopes due to diffraction, subcellular structures (typically of size $<$20nm) appear as blurred spots. Regardless of object shape, in this case, the intensity profile is modeled by a 2D Gaussian approximation of the point-spread function (PSF) of the microscope. To model the manifest elongation in the intensity profile of MTs we utilize the velocity components from the state vector $\mathbf{x}_k$ as parameters in the PSF. In this case, for an object of intensity I_k at position (x_k, y_k), the intensity contribution to pixel (i, j) is approximated as:

$$h_k(i, j; \mathbf{x}_k) = I_k \exp\left(-\frac{1}{2}\mathbf{m}^T \mathbf{R}^T \mathbf{\Sigma}^{-1} \mathbf{R}\mathbf{m}\right) + b \tag{5}$$

where b is the background intensity, $\mathbf{R} = \mathbf{R}(\phi)$ is a rotation matrix

$$\mathbf{R}(\phi) = \begin{pmatrix} \cos\phi & \sin\phi \\ -\sin\phi & \cos\phi \end{pmatrix}, \quad \mathbf{\Sigma} = \begin{pmatrix} \sigma_{\text{max}}^2 & 0 \\ 0 & \sigma_{\text{min}}^2 \end{pmatrix},$$

$$\mathbf{m} = (i\Delta_x - x_k, j\Delta_y - y_k)^T, \quad \tan\phi = \frac{\dot{y}}{\dot{x}}.$$

The parameters σ_{max} and σ_{min} represent the amount of blurring and, at the same time, model the elongation of the object along the direction of motion.

The complete measurement recorded at time k is an $N \times M$ matrix denoted as $\mathbf{z}_k = \{z_k(i, j) : i = 1, ..., N, j = 1, ..., M\}$. Since the object (if present) will affect only the pixels in the vicinity of its location (x_k, y_k), the likelihood function can be expressed as follows:

$$L_G(\mathbf{z}_k|\mathbf{x}_k) = \prod_{(i,j)\in C(\mathbf{x}_k)} p(z_k(i, j)|\mathbf{x_k}) \tag{6}$$

where $C(\mathbf{x}_k) = \{(i, j) \in \mathbb{Z}^2 : h_k(i, j; \mathbf{x}_k) - b > 0.1 I_k\}$ and

$$p(z_k(i, j)|\mathbf{x}_k) \propto \frac{1}{\sigma_\eta(i, j)} \exp\left(-\frac{(z_k(i, j) - h_k(i, j))^2}{2\sigma_\eta^2(i, j)}\right) \tag{7}$$

where $\sigma_\eta^2(i, j)$ is the variance of the measurement noise in the pixel (i, j), assumed to be independent from pixel to pixel

and from frame to frame. Poisson noise, which can be used to model the effect of the quantum nature of light on the measured data, is one of the main sources of noise in fluorescence microscopy imaging. The recursive Bayesian solution is applicable as long as the statistics of the measurement noise is known for each pixel. In this paper we used a valid approximation ($b > 100$) of Poisson noise with $\sigma_\eta^2(i,j) = h_k(i,j)$.

Generally, the likelihood $L_G(\mathbf{z}_k|\mathbf{x}_k)$ is very peaked (even when the region $C(\mathbf{x}_k)$ is small) and may lead to severe sample impoverishment, where all N_s particles occupy the same point in the state space, giving a poor representation of the posterior density. This effect is even stronger for the image data with a low SNR but in our case can be partly solved using, for example, the Auxiliary Particle Filter (if the process noise is small) or Regularized Particle Filter approaches [8]. In order to overcome such problems we also propose a second observation model

$$L_S(\mathbf{z}_k|\mathbf{x}_k) \propto \frac{1}{\sigma_\eta(\mathbf{x}_k)} \exp\left(-\frac{\left(S_k^z(\mathbf{x}_k) - S_k^o(\mathbf{x}_k)\right)^2}{2\sigma_\eta^2(\mathbf{x}_k)}\right) \quad (8)$$

where

$$S_k^z(\mathbf{x}_k) = \sum_{(i,j)\in C(\mathbf{x}_k)} z_k(i,j), \quad S_k^o(\mathbf{x}_k) = \sum_{(i,j)\in C(\mathbf{x}_k)} h_k(i,j).$$

and the variance $\sigma_\eta^2(\mathbf{x}_k)$ is taken to approximate the Poisson distribution with $\sigma_\eta^2(\mathbf{x}_k) = S_k^o(\mathbf{x}_k)$. The likelihood $L_S(\mathbf{z}_k|\mathbf{x}_k)$ is less peaked but gives an error of the same order as $L_G(\mathbf{z}_k|\mathbf{x}_k)$. Another advantage is that $L_S(\mathbf{z}_k|\mathbf{x}_k)$ can be used for objects without a predefined shape; only the region $C(\mathbf{x}_k)$, which presumably contains the object, and the total object intensity in $C(\mathbf{x}_k)$ should be specified. For the robustness and better accuracy in this case, the local curvature of the image intensity distribution can be used as an additional discriminating feature in $\mathbf{z}_k$. The measurements produced by the tracked objects are characterized by a combination of convex intensity distributions in all directions and a relatively high mean intensity. Noise-induced local maxima typically exhibit a random distribution of intensity changes in all directions leading to a low local curvature [3].

3.4. Evaluation on Synthetic Data

The performance of the particle filter was evaluated using highly realistic synthetic 2D+T images (size $512 \times 512 \times 20$, $10-20$ objects per frame) generated according to (4) and (5) for different SNRs. The velocities of the objects ranged from 200 to 700 nm/sec, representative of published data [9]. The particle filter used 10^3 samples per object and was set with the following parameters: $b = 100$, $\sigma_{\max} = 250$ nm, $\sigma_{\min} = 120$ nm, $\Delta_x = \Delta_y = 50$ nm, $q_1 = 3$ and $q_2 = 0.1$, $T = 1$ sec. Figure 2 displays intensity profiles of three generated spots with a different SNR. The SNR is calculated as the difference in intensity between the object I_o and background

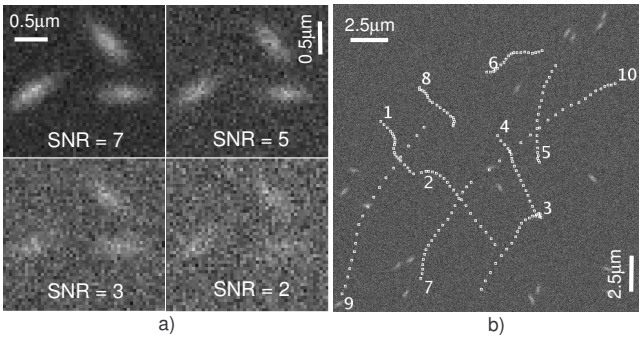

Fig. 2. (a) Intensity profiles of generated spots for different SNR; (b) Synthetic data representing 10 tracks (20 time-steps, SNR= 4).

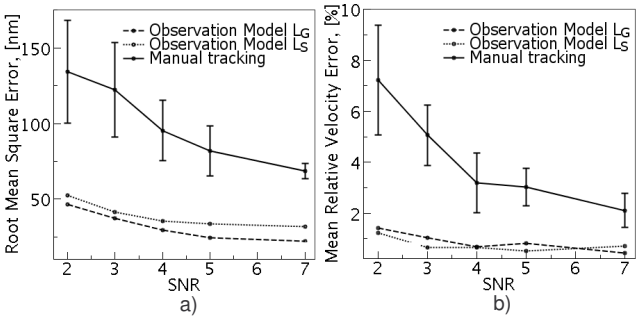

Fig. 3. (a) RMSE and (b) the mean relative velocity error as functions of the SNR for the automatic and manual tracking.

I_b divided by the noise of the object σ_o [10]. For automatic initialization, spatiotemporal ROIs [11] modified for dealing with our image data were used. The modifications help to initialize new tracks and include local object detection and the Hough transform for local track segmentation. Having the ground truth for the synthetic data, we evaluate the accuracy of the tracking and compared the PF-technique (using two proposed observational models L_G and L_S) and manual tracking (done by three independent observers). In order to quantify the localization error we use the traditional measure of performance: the Root Mean Square Error (RMSE) [11].

Figure 3 displays the RMSE and the mean relative error in the velocity estimates as functions of the SNR. The localization error for the automatic tracking is in the range of 10-50 nm which is approximately 2-3 times smaller than for the manual tracking. The error bars in Fig. 3 represent the interobserver variability in the position and velocity estimation and indicate that in the case of manual tracking the performance degrades significantly for low SNRs. The experiments also reveal that the velocity estimates obtained by manual tracking are always overestimated. For biologists it means that special care should be taken when any conclusions about or comparisons between the theoretical and experimental (based on the results of manual tracking) velocity estimates are made.

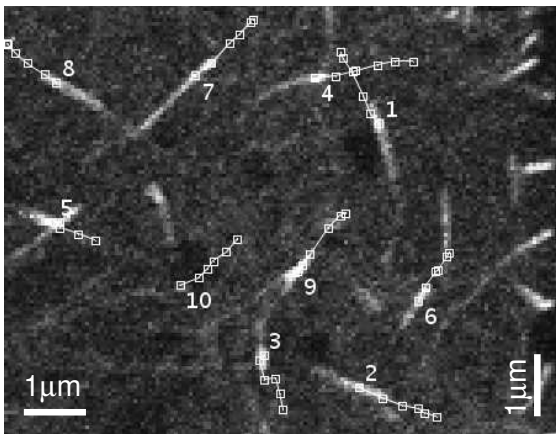

Fig. 4. Visualization of the results (10 tracks) of tracking microtubules (bright, elongated spots) using our technique (single frame from 2D time-lapse studies).

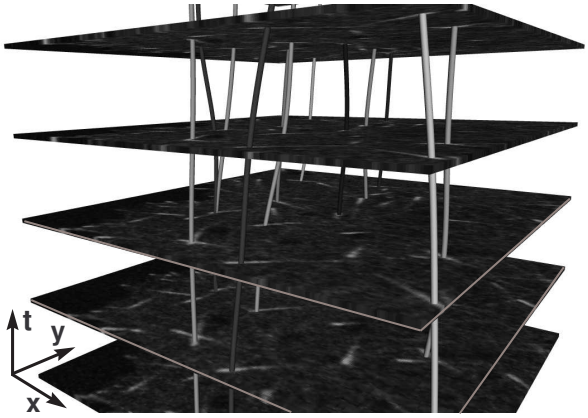

Fig. 5. Visualization of a 2D+time fluorescence microscopy image sequence showing microtubules (bright, elongated spots) and the results of tracking using our technique.

3.5. Evaluation on Real Data

We applied the method to three 2D+T data sets of growing microtubules with dimension of $512 \times 512 \times 20$. The data sets were preselected from larger volumes by manually choosing the regions of interest. In this case, the observation model L_G was used and the parameters of the particle filter were taken the same as in the case of the synthetic data. The results of tracking growing MTs are presented in Fig. 4 and Fig. 5. In the experiments the tracker simultaneously followed 10-20 spots originating from manually defined regions of interest (ROIs) during 3-10 consecutive frames until their disappearance.

The evaluation of the technique has been performed by visual inspection and by comparison with the results of manual tracking of the same spots. Lacking the ground truth for the real data, we estimated the localization error between the automatic and manual tracking. The error ranged from 180 nm (SNR=2) to 50 nm (SNR=7) which is approximately the same as in the case with the synthetic data without the ground truth.

Velocity distributions were obtained for the image data with different biological experimental conditions. Our velocity estimates are comparable to the estimates derived by means of manual tracking from the same type of image data reported in [9].

4. CONCLUSIONS

We have demonstrated the applicability of particle filtering techniques for quantitative analysis of subcellular dynamics. Compared to existing approaches in this field the method is a substantial improvement for detection and tracking of large number of spots in image data with a low SNR. Experimental result demonstrate that the automated method produces results comparable to manual tracking but using only a fraction of the manual tracking time. Currently we are undertaking a quantitative validation of the method for other biological applications in order to further demonstrate the improvements over current means of manual and automated quantification of subcellular dynamics.

5. REFERENCES

[1] E. Meijering, I. Smal, and G. Danuser, "Tracking in molecular bioimaging," *IEEE Sig. Proc. Mag.*, vol. 23, no. 3, pp. 46–53, May 2006.

[2] I. Smal, W. Niessen, and E. Meijering, "Bayesian tracking for fluorescence microscopic imaging," in *Proc. IEEE Int. Symp. on Biomedical Imaging*, Apr. 2006, pp. 550–3.

[3] D. Thomann, D.R. Rines, P.K. Sorger, and G. Danuser, "Automatic fluorescent tag detection in 3D with super-resolution: application to the analysis of chromosome movement," *J. Microsc.*, vol. 208, no. 1, pp. 49–64, 2002.

[4] B.C. Carter, G.T. Shubeita, and S.P. Gross, "Tracking single particles: a user-friendly quantitative evaluation," *Phys. Biol.*, vol. 2, pp. 60–72, Mar. 2005.

[5] J. Vermaak, A. Doucet, and P. Pérez, "Maintaining multi-modality through mixture tracking," in *Proc. 9th IEEE Int. Conf. Comp. Vis.*, 2003, pp. 1110–16.

[6] M. Isard and A. Blake, "Condensation – conditional density propagation for visual tracking," *Int. J. Comp. Vis.*, vol. 29, no. 1, pp. 5–28, 1998.

[7] Y. Bar-Shalom, X.R. Li, and T. Kirubarajan, *Estimation with Applications to Tracking and Navigation*, Wiley, New York, 2001.

[8] S.M. Arulampalam, S. Maskell, N. Gordon, and T. Clapp, "A tutorial on particle filters for online nonlinear/non-gaussian bayesian tracking," *IEEE Trans. Sig Proc.*, vol. 50, no. 2, pp. 174–88, Feb. 2002.

[9] T. Stepanova, J. Slemmer, C.C. Hoogenraad, G. Lansbergen, B. Dortland, C.I. De Zeeuw, F. Grosveld, G. van Cappellen, A. Akhmanova, and N. Galjart, "Visualization of microtubule growth in cultured neurons via the use of EB3-GFP (end-binding protein 3-green fluorescent protein)," *J. Neurosci.*, vol. 23, no. 7, pp. 2655–64, Apr. 2003.

[10] M.K. Cheezum, W.F. Walker, and W.H. Guilford, "Quantitative comparison of algorithms for tracking single fluorescent particles," *Biophys. J.*, vol. 81, no. 4, pp. 2378–88, Oct. 2001.

[11] W. Ng, J. Li, S. Godsill, and Vermaak J., "A hybrid method for online joint detection and tracking for multiple targets," *IEEE T. Aero. Elec. Sys.*, vol. 1, no. 1, pp. 1–20, Jan. 2006.